

Spectroscopic Characterization of an Argon-Neon Z-Pinch Plasma at Stagnation

K. L. Wong, P. T. Springer, J. H. Hammer, C. A. Iglesias, A. L. Osterheld, M. E. Foord, H. C. Bruns, and J. A. Emig
Lawrence Livermore National Laboratory, Livermore, California 94551

C. Deeney

Sandia National Laboratory, Albuquerque, New Mexico 87185

(Received 28 August 1997)

The density, temperature, and radiation coupling are investigated in strongly radiating Ar-Ne Z-pinch plasmas at stagnation using a novel high resolution space- and time-resolving x-ray spectrometer. One- and two-dimensional electron temperature profiles are obtained from the slope of the Ne recombination continuum. The electron density and ion temperature are determined from comparisons of the helium-like Ar Rydberg series with detailed line-profile calculations. 2D nonlocal thermodynamic equilibrium calculations predict a radiating region denser and cooler than measured. [S0031-9007(98)05535-5]

PACS numbers: 52.55.Ez, 52.50.Lp, 52.70.La

The hot, dense radiating plasmas produced in high power Z-pinch implosions have a wide variety of applications, ranging from materials testing, x-ray lithography, and microscopy [1] to the spectroscopy of highly charged ions [2,3]. At drive powers of 10 TW and above, a pinch x-ray source can heat materials to black body temperatures of order 100 eV for applications in high energy density physics [4]. Many of these applications require a higher energy density than achieved to date with Z pinches, e.g., by a factor of ~ 100 for inertial confinement fusion, placing a premium on understanding and controlling pinch dynamics that limit the achievable energy density. At present, there is very limited understanding of Z-pinch dynamics, with no "first-principles" calculation of an imploding pinch that agrees with observations. One-dimensional (radius and time) magnetohydrodynamic (MHD) models predict radiative collapse to micron dimensions and subnanosecond x-ray pulses, in disagreement with experiments [5]. Attempts to force pulse-width agreement with one-dimensional calculations require *ad hoc* transport multipliers or modification of the hydrodynamics [6]. The imploding sheath is magneto-Rayleigh-Taylor (RT) unstable, and two-dimensional models (r, z, time) can reproduce the observed x-ray pulse widths [5,7], although they employ *ad hoc* assumptions of the RT seed level. The RT instability is a primary reason for the modeling difficulty since unstable modes undergo many e -foldings leading to strong nonlinearity. In addition, and depending on the pinch parameters, it may be necessary to use nonlocal thermodynamic equilibrium (non-LTE) models for the plasma ionization state and radiative properties, include the effect of lower hybrid drift turbulence on plasma resistivity, or include non-MHD Hall-type effects. In view of the difficulties in accurately predicting pinch output, a clear need exists for well characterized measurements to test current models.

Previous time- and space-resolved measurements used grating spectrometers in the visible [8] and XUV range [9,10], and only estimates of the plasma conditions were

obtained. Time-integrated and time-resolved x-ray crystal spectroscopy have been used to determine plasma temperatures and densities using line-ratio techniques [10,11]. However, the results are either temporally averaged over the entire implosion or over a 10 ns time frame where the conditions may change rapidly. In this Letter, we report the first detailed, space- and time-resolved measurements of the density and temperature of a stagnating high current Z-pinch and compare the observations with 2D non-LTE radiation MHD calculations.

The experiments were performed at the SATURN facility at Sandia National Laboratory [12]. Highly ionized Ne-Ar plasmas are formed by first injecting 300 $\mu\text{g}/\text{cm}$ annular or 100 $\mu\text{g}/\text{cm}$ uniform 90% Ne-10% Ar neutral gas columns into the 5×10^{-5} torr vacuum between the anode and cathode of the device. UV flashboards preionize the gas, and SATURN is fired 1 μs later delivering ~ 8 MA at 1.9 MV to the load. The $\mathbf{J} \times \mathbf{B}$ force drives the plasma inward at velocities near 8×10^7 cm/s. The plasma stagnates on axis in 60-90 ns as the plasma kinetic energy is transferred to x rays.

A schematic of the experimental setup is shown in Fig. 1. A high resolution, radially imaging, Johann curved-crystal spectrometer monitors the x-ray emission. A 10 cm long ADP(101) and quartz(110) crystals, bent to radii of curvature of 50 cm, produce spectrally dispersed 1D images with a magnification of 1.7 and a resolving power of order 3000. The total x-ray energy range covered is 1.6-2.0 keV for the ammonium-dihydrogen-phosphate (ADP) crystal and 3.4-4.4 keV for the quartz crystal at a nominal Bragg angle of 40° . A 1 cm long ADP(101) and quartz(110) crystals, bent to radii of curvature of 88 cm, produce 2D monochromatic images of the plasma. The Bragg angles for the ADP and quartz crystals are set independently to 35° and 42.5° and demagnify 7.7 and 4.6, respectively, in the axial direction. X rays are recorded on a two-dimensional gated microchannel plate (MCP) detector with three active striplines which can be biased to different voltages coupled to a phosphor coated fiber optic

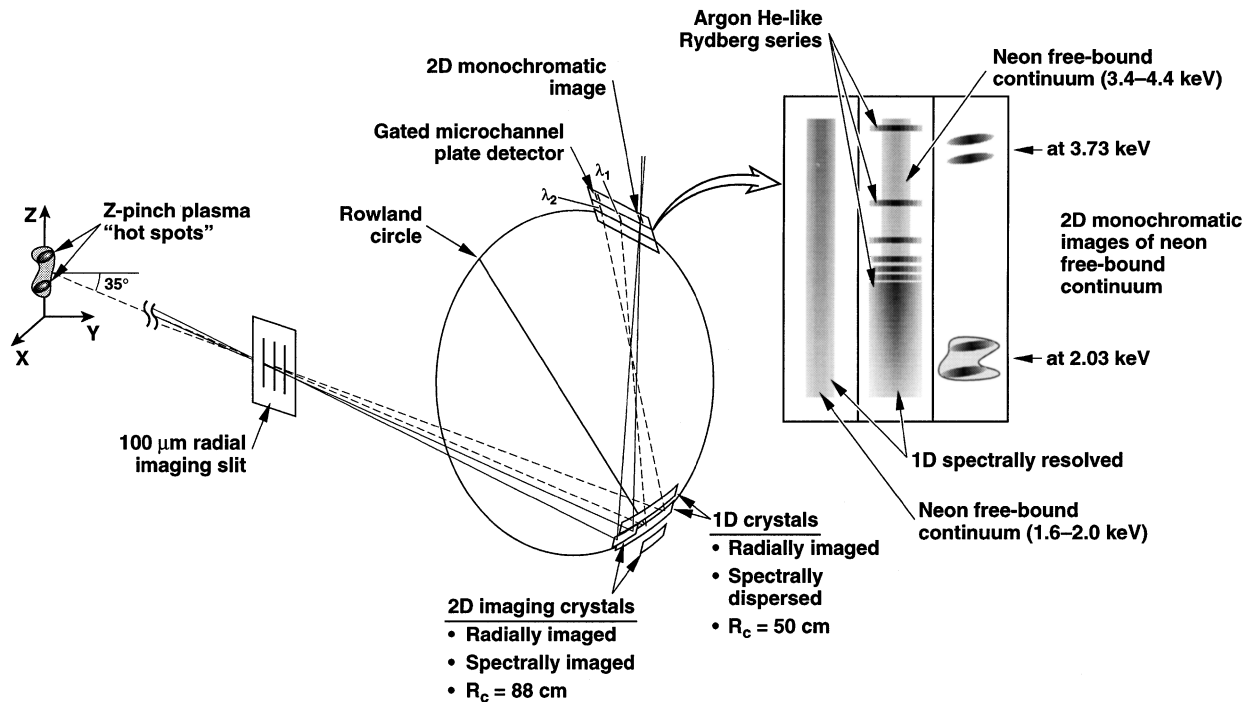


FIG. 1. Schematic drawing of the experimental setup.

plate. The MCP, coated with a Au photocathode, is active for 2 ns of the typical 20 ns x-ray pulse of SATURN. The data were recorded on Kodak optical TMAX film. A microdensitometer measured the film optical density versus position. Each piece of film was developed with a pre-exposed calibrated step wedge to convert optical density to x-ray exposure.

Figure 1 shows an illustration of typical film data from an Ar-Ne shot. The broad band exposure running across the left strip represents radiative recombination continuum onto fully ionized neon ions. Lines on the middle strip illuminated by the quartz crystal are the heliumlike and hydrogenic Ar Rydberg series. Line emission from the heliumlike ($n = 1-3$) to the heliumlike ($n = 1-9$) and hydrogenic ($n = 1-3$) to the hydrogenic ($n = 1-9$) where n is the principal quantum number are resolved. Superimposed on the line series is the Ne free-bound continuum radiation. The right strip shows the monochromatic 2D plasma images from the ADP (bottom) and the quartz (top) crystals of the Ne free-bound continuum at 2.03 and 3.73 keV, respectively.

A number of other time-resolving diagnostics were fielded for the Ar-Ne Z-pinch implosion experiments. Rogowski coils and B-dot probes monitored the peak and total current delivered to the load as a function of time. A Ni bolometer gave time-resolved information on the total x-ray yield of the plasma, and a set of four filtered photoconducting detectors (PCD) gave time histories of the radiation pulse width [13]. A time-resolved large format pin-hole camera (LFPHC) which takes nine images of the plasma 2 ns apart gave 2D spatial information of the plasma evolution [5,14].

The electron temperature is obtained from the slope of the free-bound continuum radiation for optically thin plasmas. The calculated opacities for the Ne-Ar continua give optical depths of $0.1-1.0 \text{ cm}^{-1}$ for a 16% Ar-84% Ne plasma at a density of 0.08 g/cm^3 and electron temperature of 1200 eV. The slope is computed by taking the ratio of the recombination x-ray intensities $I(E)$ and $I(E + \Delta E)$, where E is the photon energy, and using the intensity ratio $I(E)/I(E + \Delta E) = \exp(\Delta E/kT_e)$ for a Maxwellian electron velocity distribution [15,16] where the ratio of the Gaunt factors is close to unity [17]. The intensity ratios are corrected for absolute spectrometer efficiency of each crystal, Be-filter transmission, MCP detector gating response, film sensitivity, x-ray transmission through the gas column, and magnification difference for the ADP and quartz imaging crystals. The spectrometer was absolutely calibrated using Au bremsstrahlung x rays produced by a Manson source.

We obtain 2D electron temperature maps by taking radial and axial projections of the Ne free-bound continuum. The radial projections of the Ne free-bound radiation are derived from the ADP crystal data (left strip in the Fig. 1 data illustration) at an x-ray energy of 1.7 keV and from the quartz crystal at 3.7 keV (middle strip in the Fig. 1 data illustration). Similarly, axial projections of the 2D monochromatic Ne free-bound images are derived from the right strip of the Fig. 1 data illustration. Results are shown in Figs. 2(a) and 2(c) for an annular fill plasma. Ratios indicate that the peak radial and axial electron temperatures are $1.25 \pm 0.18 \text{ keV}$ for the annular fill plasma as shown in Figs. 2(b) and 2(d) and $1.6 \pm 0.24 \text{ keV}$ for the uniform fill plasma. The uniform fill plasmas have

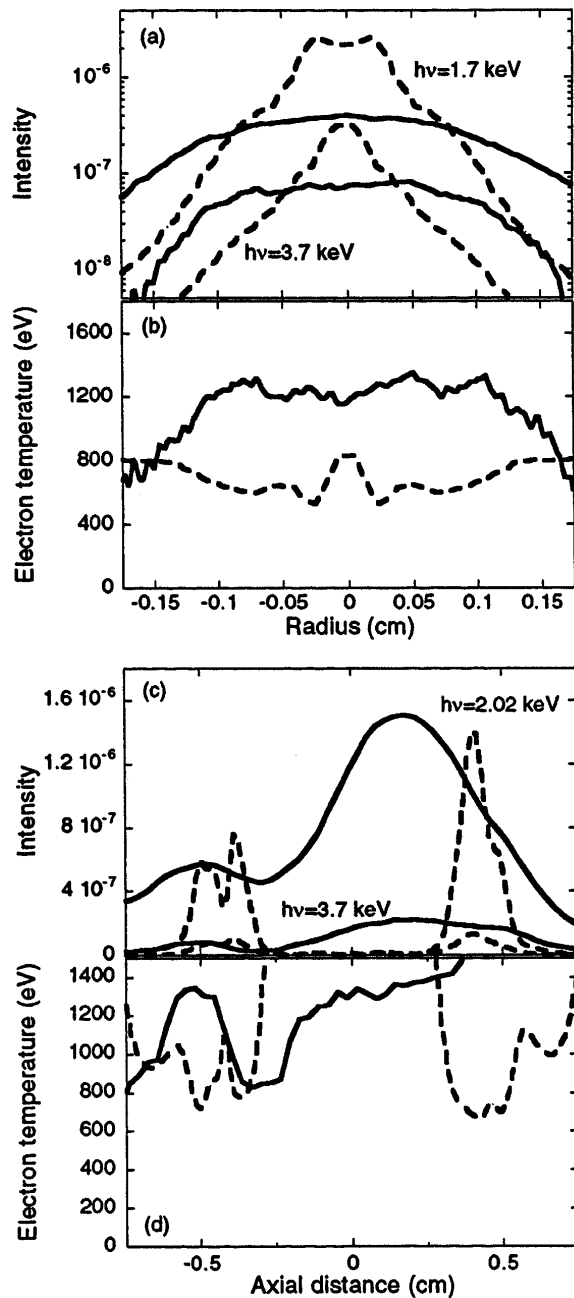


FIG. 2. Comparison of the radial and axial profiles (a) and (c) and electron temperatures (b) and (d) for the data (solid lines) and a 2D non-LTE radiation MHD calculation (dashed lines). The radial profiles were measured at photon energies of 1.7 keV (top curve) and 3.7 keV (bottom curve), and the axial profiles were measured at photon energies of 2.02 keV (top curve) and 3.7 keV (bottom curve).

less mass and thus implode at faster speeds and stagnate on axis at higher electron temperatures.

The electron density, ion density, and ion temperature are determined from a fit to the heliumlike Ar Rydberg series. A Gaussian least-squares fit was applied to the data as in Fig. 3 in which the width consisted of two components. One component was assumed to be thermal Doppler broadening. The other is due to Stark broadening in which the

width of the lines was assumed to vary as $n^2 n_e^{2/3}$ where n is the principal quantum number of the upper level in the Rydberg transition. The Doppler component corresponds to an ion temperature of 36 ± 7.2 keV. To determine the electron density we compare the experimental Stark widths to results from the TOTAL code [18] using HULLAC [19] generated matrix elements and a 2-temperature microfield distribution. We determine an axially averaged electron density of $(0.8 \pm 0.2) \times 10^{21}$ cm $^{-3}$ for the annular gas puff. Assuming this electron density and a plasma consisting of 90% Ne $^{10+}$ and 10% Ar $^{16+}$ yields a mass density of 0.0028 ± 0.0007 g/cm 3 .

We have compared our results to both 2D radiation MHD local thermodynamic equilibrium (LTE) simulations [5] and non-LTE calculations. In the non-LTE case, the atomic physics is treated with a time-dependent average atom-model, while for the LTE case, a Thomas-Fermi model is employed. Our simulations show magneto-Rayleigh-Taylor instabilities and axial inhomogeneities strongly develop from initial perturbations in the density profile and have a dominant effect on x-ray pulse width. LFPHC images show that the measured 20 ns time duration of the x-ray burst is due to plasma zippering [14] where the characteristic lifetime for an emission "hot spot" is the sheath width/implosion velocity ~ 2 ns. The models also account for the possibility of the sausage instability which is not seen at stagnation but may occur at later times. A sequence of density and electron temperature profiles just prior to and including stagnation is shown in Fig. 4 for the non-LTE calculation. The data correspond to a time of 104 ns in this simulation. With a 1% initial random zone to zone density perturbation seeding the Rayleigh-Taylor instability and 25% initial smooth axial variation to cause zippering, x-ray pulse widths and total radiation yields are in reasonable agreement with the measurements. However, both LTE and non-LTE models predict higher densities, smaller radii, and lower temperatures at stagnation compared with the experiment. The 2D LTE calculation predicts a stagnation density of 0.33 g/cm 3 , electron temperature of 300 eV, and a FWHM pinch diameter of 200 μ m compared with 2 mm for the experiment. The 2D non-LTE model gives an improved stagnation density of 0.018 g/cm 3 with a FWHM pinch diameter of 0.5 mm and

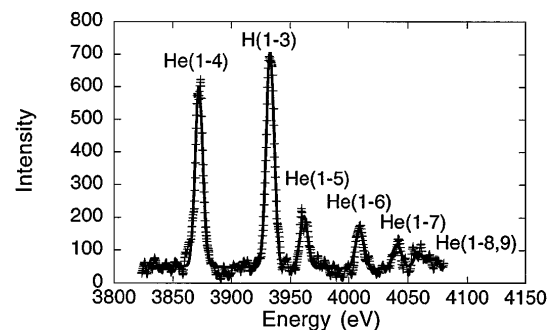


FIG. 3. A two component fit to the He-like Ar Rydberg series for an annular fill shot.

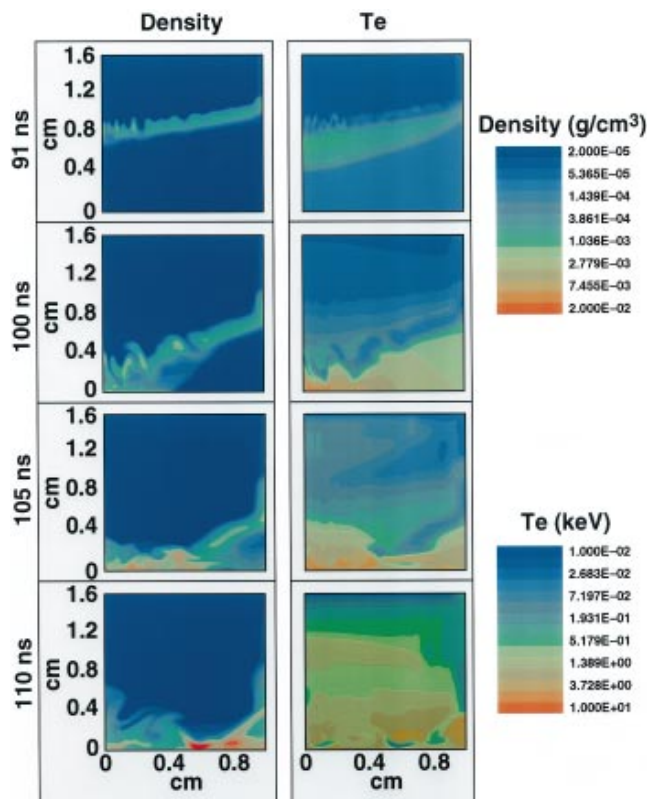


FIG. 4(color). The density and electron temperature evolution of a 2 cm long, 1.25 cm radius, and 0.8 cm annular 90% Ne–10% Ar plasma sheath. The maximum current was 8 MA. The axial variation was $300 \mu\text{g}/\text{cm}$ in the middle and $375 \mu\text{g}/\text{cm}$ on the ends with a 1% initial density perturbation.

an electron temperature of 700 eV as shown in Figs. 2(b) and 2(d). In both models the plasma radiatively cools during the implosion with significantly greater radiation loss in the LTE case, giving cooler electron temperatures, stronger coupling to the ions, and higher density pinches. The final predicted temperatures in both cases are too low to produce the H-like Ar ionization state experimentally observed.

The energetics of the shock heated plasma column at stagnation were investigated through a series of 1D non-LTE calculations in which 200 kJ of energy was uniformly deposited in fixed cylinders of 10% Ar and 90% Ne. The radii were varied from 0.4 to 0.04 cm, and the energy input times were scaled proportionally with radius from 16 to 1.6 ns, respectively, consistent with a shock speed of 10^7 cm/s . The final density, electron and ion temperatures, average ionization state, and radiated energy were then calculated. At small radii, the temperature and density match the 2D non-LTE simulation values, while at the experimentally observed radius (2 mm), the density and electron temperature agree well with the experiment. The calculated ion temperature (a few keV) for both 1D and 2D simulations is much lower than experimentally observed. However, the 2D simulations give an emission averaged flow energy several tens of keV, suggesting that the Doppler temperature ($\sim 36 \text{ keV}$) may be strongly affected by plasma flow. Thus, the discrepancy between

modeling and experiment may be due to the exclusion of additional physics governing the hydrodynamics of the radial convergence. 3D effects such as convective mixing and angular rotation or small scale turbulence could, for example, prevent the plasma from reaching the high densities.

In conclusion, we have measured with high spectral-, spatial-, and time resolution the plasma conditions of a high powered Z pinch at stagnation. 2D electron temperature profiles were inferred from the Ne recombination continuum. Electron densities and ion temperatures were determined from comparisons with heliumlike Ar line broadening calculations. With known initial input parameters and high precision measurements of the plasma conditions at stagnation, both LTE and non-LTE 2D radiation MHD models were compared with the data. We find the simulations correctly predict the total radiated power but predict plasmas that are too dense, tightly pinched, and cool at stagnation. This lack of agreement has important implications in limiting the utility of predicting energy densities, temperatures, powers, x-ray yields, and charge states attainable on Z-pinch plasmas. Further work is required to resolve these discrepancies.

We wish to thank A. Toor, M.K. Matzen, and M. Eckart for their support of the experiment, and the SATURN PRS crew for their technical assistance. This work was performed under the auspices of the U.S. Department of Energy by Lawrence Livermore National Laboratory and Sandia National Laboratories under Contracts No. W-7405-ENG-48 and No. DE-AC04-94AL85000.

- [1] N. R. Pereira and J. Davis, *J. Appl. Phys.* **64**, R1 (1988).
- [2] R. E. Stewart *et al.*, *J. Appl. Phys.* **61**, 126 (1987).
- [3] R. E. Stewart *et al.*, *J. Opt. Soc. Am. B* **4**, 396 (1987).
- [4] M. K. Matzen, *Phys. Plasmas* **4**, 1519 (1997).
- [5] J. H. Hammer *et al.*, *Phys. Plasmas* **3**, 2063 (1996).
- [6] J. W. Thornhill *et al.*, *J. Appl. Phys.* **80**, 710 (1996).
- [7] D. L. Peterson *et al.*, *Phys. Plasmas* **3**, 368 (1996).
- [8] M. E. Foord *et al.*, *Phys. Rev. Lett.* **73**, 1190(E) (1994).
- [9] R. E. Marrs *et al.*, *Appl. Phys. Lett.* **42**, 946 (1983).
- [10] T. Nash *et al.*, *J. Quant. Spectrosc. Radiat. Transfer* **44**, 485 (1990).
- [11] C. Deeney *et al.*, *Phys. Rev. E* **51**, 4823 (1995).
- [12] D. D. Bloomquist *et al.*, in *Proceedings of the 6th International Electrical and Electronic Engineering Pulsed Power Conference, Arlington, VA*, edited by P. J. Turchi and B. H. Bernstein (IEEE, New York, 1987), p. 310.
- [13] C. Deeney *et al.*, *Phys. Plasmas* (to be published).
- [14] M. R. Douglas *et al.*, *Phys. Rev. Lett.* **78**, 4577 (1997).
- [15] B. K. F. Young *et al.*, *Phys. Rev. Lett.* **61**, 2851 (1988).
- [16] C. DeMichelis and M. Mattioli, *Nucl. Fusion* **21**, 677 (1981).
- [17] W. J. Karzas and R. Latter, *Astrophys. J. Suppl.* **55**, 167 (1961).
- [18] A. Calisti *et al.*, *Phys. Rev. A* **42**, 5433 (1990).
- [19] A. Bar-Shalom and M. Klapisch, *Comput. Phys. Commun.* **50**, 375 (1988).